An Empirical Potential Energy Surface for the He−Br_2 ($B^3\Pi_u$) van der Waals Complex

A. García-Vela*

Instituto de Matemáticas y Física Fundamental, C.S.I.C., Serrano 123, 28006 Madrid, Spain

Received: March 7, 2005; In Final Form: May 6, 2005

An empirical potential energy surface is proposed for the He−Br_2 ($B^3\Pi_u$) complex. The intermolecular potential is modeled as a sum of pairwise He−Br Morse interactions plus a three-body interaction term. The parameters of the potential are fitted in order to reproduce the spectral blue-shifts and vibrational predissociation line widths measured for He−$^{79}Br_2$ (B, v') in the range $v' = 8-48$ of Br_2 vibrational excitations. The calculated blue-shifts and line widths are in very good agreement with the measurements (typically within experimental error or close to its limits) along the whole range of v' levels studied. It is particularly remarkable to note the accuracy provided by the interaction surface in the region of high v' excitations ($v' > 35$), where three-body effects become important. The behavior of the potential surface with the Br−Br separation is analyzed and correlated with the experimental findings.

I. Introduction

The spectroscopy and photodissociation dynamics of rare-gas−halogen van der Waals (vdW) complexes have been extensively studied over the last two decades. Such complexes are ideal systems to investigate energy transfer processes, intramolecular vibrational redistribution (IVR) mechanisms, and weak vdW interactions. A wide variety of complexes of different rare-gas atoms (He, Ne, Ar) weakly bound to molecules such as I_2,[1−13] Cl_2,[14−23] ICl,[18b,24−26] and Br_2,[27−33] have been studied. Much of the research effort has focused on the simplest triatomic systems. Among them, the He−Br_2 complex has been the subject of a number of experimental works. The He−Br_2 B(v') ← X($v'' = 0$) transition was probed in the region $v' = 8-48$ of Br_2 vibrational excitations, for He−$^{79}Br^{81}Br$ (ref 27) and He−$^{79}Br_2$.[27−29,32] Excitation spectra, spectral blue-shifts of the He−Br_2 B(v') ← X($v'' = 0$) band origins from the corresponding Br_2 B(v') ← X($v'' = 0$) band origins, line widths of vibrational predissociation (VP), and product rotational state distributions of the Br_2 fragment produced upon VP were measured. Such a large collection of experimental data, probing a wide range of the Br_2 spectrum of vibrational levels, provides an ideal testing ground to characterize the potential energy surfaces associated with the He−Br_2 interaction.

Several potential surfaces have been proposed for the ground electronic state X of He−Br_2, including empirical[29,30] and ab initio[34] ones. A number of surfaces were also reported for the He−Br_2 excited electronic state B, like empirical ones based on a sum of atom−atom Morse potentials,[29,30] a diatomics-in-molecule (DIM) potential surface,[33] and a recent ab initio surface.[35] Among the B-state potentials, the empirical surface of ref 30 has been the one most extensively tested against the experimental data. This potential reproduces the rotational distributions of the Br_2 fragment produced after VP in good agreement with the measured ones.[32] Likewise, the experimental spectral blue-shifts and line widths are well-described by the potential up to $v' \simeq 38$.[30] However, the description of these quantities for higher vibrational excitations is less satisfactory. The experiment[27−29] finds that the spectral blue-shift increases up to $v' \approx 35$, and then, it decreases for higher v', which suggests that the vdW bond becomes stronger for large Br−Br separations (>4.0 Å).[28] This behavior is not reproduced by the empirical potential, which overestimates the blue-shifts for $v' > 36$ and predicts a complicated oscillatory behavior in this region.[30] In turn, the VP line widths are typically underestimated by the potential surface for $v' > 38$, as compared with the experimental ones.[28]

It was found in ref 30 that for $v' \geq 38$ the He−Br_2 (B, v') resonance initially excited strongly interacts with several metastable states belonging to lower vibrational manifolds $v < v'$, which complicates the description of the VP process for high v' excitations. In addition, the trend inversion of the spectral shifts found experimentally for $v' > 35$ seems to indicate an important dependence of the potential surface on the Br−Br separation, particularly as this separation increases approaching the Br_2 dissociation limit. The poor representation in the empirical pairwise potential of such a dependence and the three-body effects involved could explain much of the disagreement with experiment for high v' levels. Indeed, in a later work,[33] a first-order DIM-based potential surface was reported, containing a three-body term through which a dependence on the Br−Br separation was taken into account. The spectral shifts obtained with this potential decreased, improving substantially[33] in the region of high Br_2 vibrations with respect to previous results,[30] although still displaying an oscillatory pattern. The improvement was mainly attributed to the dependence on the Br−Br separation introduced. The VP line widths for high v' were not examined with this potential.

The above works indicate that, in order to describe correctly the spectroscopy and dynamics of He−Br_2 (B, v') in the whole range of v' probed experimentally, the dependence on the interhalogen separation must be properly represented in the potential surface by including three-body effects. A similar situation has been found for the related He−Cl_2 (B, v') complex. In this case, the vibrational dependence of the VP lifetimes measured in the range $v' = 8-12$ (ref 19) was poorly described by empirical pairwise potential surfaces. In a recently proposed He−Cl_2 (B) empirical surface,[22] a three-body character was introduced by making some of the potential parameters explicitly

* E-mail: garciavela@imaff.cfmac.csic.es.

10.1021/jp051167n CCC: $30.25
Published on Web 06/04/2005

dependent on the Cl−Cl bond distance. As a result, the description of the vibrational dependence of the lifetime was substantially improved.

The ab initio He−Br_2 (B) potential reported in ref 35 was calculated for three Br−Br separations between 2.4 Å and 3.1 Å, and therefore, it does not sample the region of high v' states. Even today, highly accurate ab initio calculations for an excited state of a system with so many electrons such as He−Br_2 are not straightforward. They are complicated further as the Br−Br separation increases, because of possible crossings between the ab initio adiabatic potentials. In this situation, an empirical fit of the He−Br_2 (B) potential surface becomes an alternative, provided that enough data are available. The aim of the present work is to extend the model successfully applied to He−Cl_2 (B) to the He−Br_2 (B) complex, to characterize a potential surface able to describe the spectral shifts and predissociation line widths in the whole range of Br_2 vibrations explored experimentally.

The paper is organized as follows. In section II, the potential energy surface proposed is described, along with the details of the calculations carried out to reproduce the experimental data. In section III, the results are presented and the features of the potential surface are discussed. Section IV is devoted to conclusions.

II. Methodology

A. Potential-Energy Surface. The He−Br_2 complex is represented in (r, R, θ) Jacobi coordinates, where r is the Br−Br bond length, R is the distance between He and the Br_2 center-of-mass, and θ is the angle between the vectors **r** and **R** associated with the two radial coordinates. The He−Br_2 (B) surface is modeled as a sum of three two-body interactions plus a three-body interaction term

$$V(r, R, \theta) = V_{Br_2}(r) + V_{He-Br}(x_1) + V_{He-Br}(x_2) + V_{3B}(r, x_1, x_2) \quad (1)$$

where x_i denotes the He−Br distances

$$x_{1,2} = \left[\frac{r^2}{4} + R^2 \pm rR\cos(\theta)\right]^{1/2} \quad (2)$$

The $V_{Br_2}(r)$ term is the intramolecular Br−Br potential in the B electronic state, which is represented by a splines fit to the RKR potential of Barrow et al.[36] The $V_{He-Br}(x_i)$ terms describe the He−Br interactions, represented by a Morse potential

$$V_{He-Br}(x_i) = \epsilon_0\{\exp[-2\alpha_0(x_i - x_0)] - 2\exp[-\alpha_0(x_i - x_0)]\} \quad (3)$$

where ϵ_0, α_0, and x_0 are the three Morse parameters.

The three-body interaction term is modeled as the sum of two Morse functions of x_1 and x_2, respectively, where the Morse parameters are explicit functions of r

$$V_{3B}(r, x_1, x_2) = W(r, x_1) + W(r, x_2) = \epsilon(r)\sum_{i=1}^{2}\{\exp[-2\alpha(r)(x_i - x_m(r))] - 2\exp[-\alpha(r)(x_i - x_m(r))]\} \quad (4)$$

In addition to its simplicity, the above form for $V_{3B}(r, x_1, x_2)$ has the advantage that it reflects the symmetry in the interaction between the He atom and the two Br atoms. It is noted that the functional form of $V(r, R, \theta)$ in eq 1 is the same as that of the potential surface of ref 30 if the three-body term is neglected.

TABLE 1: Potential Parameters and Atomic Masses Used in This Work

$\epsilon_0 = 16.68$ cm^{-1}	$a_2 = 3.779$ Å^{-1}
$\alpha_0 = 1.55$ Å^{-1}	$a_3 = 0.607$ Å^{-2}
$x_0 = 3.91$ Å	$r_1 = 7.10$ Å
$\epsilon_1 = 8.2$ cm^{-1}	$r_2 = 4.00$ Å
$\alpha_1 = 0.35$ Å^{-1}	$r_3 = 5.65$ Å
$x_3 = 0.335$ Å	$m_{Br} = 79.909$ amu
$a_1 = 0.275$ Å^{-2}	$m_{He} = 4.003$ amu

The trends found experimentally and the previous theoretical works provide a useful guide to model the functional forms for $\epsilon(r)$, $\alpha(r)$, and $x_m(r)$. In this sense, the results of ref 30 indicate that representing the potential surface by a sum of two-body interaction terms only leads to a good description of the spectral shifts and line widths up to $r \approx 4.0$ Å (i.e., $v' \leq 35$). For larger Br−Br distances, a stronger r dependence related to increasing three-body effects appears to be required in the potential representation. The decrease of the spectral shifts found in the data for high v' suggests that the effect of the three-body term should be an increasing stabilization of the potential with increasing r. The above features are reflected in the following functional forms

$$\epsilon(r) = \epsilon_1 \exp[-a_1(r - r_1)^2] \quad (5)$$

$$\alpha(r) = \alpha_0 \text{ if } r \leq r_2 \quad (6a)$$

$$\alpha(r) = \alpha_0 - \alpha_1 \exp[-a_2(r - r_2)]\{\exp[-a_2(r - r_2)] - 2\} - \alpha_1 \text{ if } r > r_2 \quad (6b)$$

and

$$x_m(r) = x_0 + x_3 \exp[-a_3(r - r_3)^2] \quad (7)$$

The twelve relevant parameters ϵ_0, α_0, x_0, ϵ_1, α_1, x_3, a_j, and r_j ($j = 1-3$) are listed in Table 1. The behavior of the $\epsilon(r)$, $\alpha(r)$, and $x_m(r)$ functions is displayed in Figure 1. In the bottom panel of this figure, the (squared) vibrational eigenfunctions of Br_2 corresponding to $v' = 8$ and $v' = 48$ are also plotted to show the range of Br−Br bond lengths probed by the experiment.

The following points should be stressed: The parameters ϵ_0, α_0, and x_0 of the two-body terms are similar to those used in ref 30. Since the three-body interaction term becomes effective for $r > 3.0$ Å (see the top panel of Figure 1), the present He−Br_2 (B) potential surface is very similar to that of ref 30 for $r < 4.0$ Å, the differences arising as the interhalogen distance increases. On the other hand, the functional form of $\epsilon(r)$ causes the three-body interaction to increase gradually with r, reaching a maximum at 7.1 Å, and then vanishing as r keeps increasing. Thus, the asymptotic behavior of the potential for very large Br−Br separations approaches that of an isolated He−Br interaction, as expected.

B. Spectroscopic and Dynamical Calculations. The parameters of the He−Br_2 (B) intermolecular potential were adjusted in order to reproduce the available measurements of the spectral shifts and VP line widths in the range $v' = 8-48$ of Br_2 vibrational excitations. In the spectroscopic and dynamical calculations described in the following, total angular momentum $J = 0$ was assumed for the system. All the calculations were carried out for the He−$^{79}Br_2$ isotopic form of the complex.

The blue-shift of the He−Br_2 B(v') ← X($v'' = 0$) band origins is obtained as the difference between the corresponding dissociation energies, $D_0(X, v'' = 0) - D_0(B, v')$. The dissociation

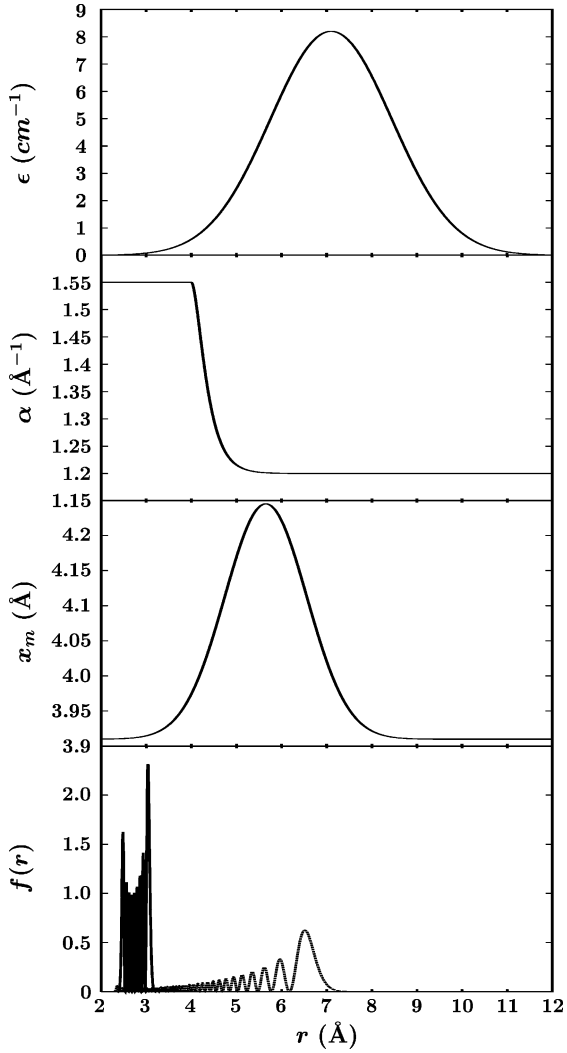

Figure 1. Behavior of the ϵ, α, and x_m functions of eqs 5−7 vs the Br−Br distance r. The Br_2 vibrational wave functions $|\chi_{v'}^{(j=0)}(r)|^2$ are also shown in the lower panel for $v' = 8$ (solid line) and $v' = 48$ (dashed line).

energy $D_0(X, v'' = 0) = 17.573$ cm^{-1} calculated in ref 30 has been used here. This energy is in good agreement with the experimental estimate of 17.0 ± 1.5 cm^{-1}.[28] The $D_0(B, v')$ binding energy is the energy of the ground resonance state of He−Br_2 (B, v'). To calculate this resonance energy, the corresponding wave function is expressed as

$$\Phi(r, R, \theta) = \sum_{n,j} c_{n,j}^{(v)} \psi_n^{(v)}(R) \chi_v^{(j)}(r) P_j(\theta) \qquad (8)$$

with $\chi_v^{(j)}(r)$ being the rovibrational eigenstates of Br_2, $P_j(\theta)$ the normalized Legendre polynomials, and $\psi_n^{(v)}(R)$ the radial basis functions. The radial functions are obtained by calculating the eigenfunctions of the reduced Hamiltonian $\hat{H}_{vv}(R, \theta) = \langle \chi_v^{(j=0)}(r)| \hat{H}|\chi_v^{(j=0)}(r)\rangle$ ($\hat{H}$ being the full Hamiltonian of He−Br_2 (B)) for several fixed angles θ and then orthogonalizing these eigenfunctions through the Gram−Schmidt procedure. The resonance energy and wave function are obtained once the Hamiltonian $\hat{H}$ is represented in the basis set of eq 8 and diagonalized. Converged resonance energies were calculated by including in the basis set 1 vibrational state $v = v'$, 10 $\psi_n^{(v)}$ radial functions, and 15 Legendre polynomials (with even j).

The vibrational predissociation line widths are obtained from simulations of the decay dynamics of the complex ground resonance state, He−Br_2 (B, v') → He + Br_2 (B, $v < v'$). In the simulations, the time-dependent Schrödinger equation is solved for the wave packet $\Phi(r, R, \theta, t)$, which is expanded as

$$\Phi(r, R, \theta, t) = \sum_{v,j} C_{v,j}(R, t) \chi_v^{(j)}(r) P_j(\theta) \exp[-E_v^{(j)} t/\hbar] \qquad (9)$$

where $E_v^{(j)}$ are the energies associated to the $\chi_v^{(j)}$ states. The expansion coefficients $C_{v,j}(R, t)$ are propagated through a set of time-dependent coupled equations. To this purpose, the $C_{v,j}(R, t)$ packets were represented on a uniform grid in the R coordinate consisting of 128 points with $R_0 = 3.0$ au and $\Delta R = 0.25$ au. In the expansion of eq 9, 15 rotational states (with even j) were included for all the dynamical calculations. Regarding the vibrational basis, 4 vibrational states corresponding to $v = v'$, $v' - 1$, $v' - 2$, and $v' - 3$ were included for the initial excitations $v' < 40$, while 5 vibrational states (adding $v = v' - 4$ to the above states) were used for $v' = 41-44$ and 6 vibrational states (adding $v = v' - 5$ to the above states) were used for $v' \geq 45$. The wave packet was absorbed before reaching the edges of the R grid. Absorption was carried out after each propagation time step by multiplying each $C_{v,j}(R, t)$ packet by the function $\exp[-A(R - R_{abs})^2]$ for $R > R_{abs}$, with $A = 0.5$ au^{-2} and $R_{abs} = 28.0$ au.

The $C_{v,j}(R, t)$ packets were propagated using the Chebychev polynomial expansion method to express the evolution operator, with a propagation time step $\Delta t = 0.04$ ps. The wave packet was propagated until a different final time t_f depending on the initial level v' being excited: $t_f = 20$ ps for $v' < 35$, $t_f = 16$ ps for $v' = 35-43$, $t_f = 12$ ps for $v' = 44$, and $t_f = 6$ ps for $v' > 44$. From the wave packet propagation up to a time t_f, the time evolution of the square of the wave packet autocorrelation function $P(t) = |\langle\Phi(0)|\Phi(t)\rangle|^2$ can be obtained until a time $2t_f$.[37] By fitting the decay curve $P(t)$ to an exponential law $P(t) \simeq e^{-t/\tau}$, the predissociation lifetime τ of the He−Br_2 (B, v') resonance state is obtained, and from τ, the resonance line width Γ can be extracted as $\Gamma = \hbar/\tau$.

Vibrational distributions of the Br_2 fragment were calculated as previously described,[38] considering that the vdW bond is effectively broken for $R > R_c = 16.0$ au. In addition, rotational state distributions of the Br_2 (B, $v < v'$, j) product fragment were computed.[22] The Br_2 rotational distributions calculated here are found to be typically colder than the experimental ones. As previously shown,[32] in order to describe theoretically the experimental rotational distributions, transitions involving $J > 0$ states must be considered in the calculations, along with proper thermal averaging over those transitions. Such $J > 0$ wave packet calculations are beyond the scope of the present work, and thus, reproduction of the measured Br_2 rotational distributions was not attempted when fitting the potential parameters.

III. Results and Discussion

A. Spectral Shifts. Analysis of the ground resonance wave functions calculated with the present potential surface shows that, in the whole range $v' = 8-48$, the wave functions are localized around $\theta = 90°$, in the perpedicular configuration of the complex. The calculated ground resonance energies of He−$^{79}Br_2$ (B, v'), E_{res}^{calc}, are listed in the third column of Table 2. The spectral blue-shifts obtained from these energies [$D_0(B, v') = -E_{res}^{calc}$] are collected in the fourth column of the table. In the last two columns, the blue-shifts measured for He−$^{79}Br_2$ are presented with the reported errors.[27−29] Only the experimental blue-shifts corresponding to the first open VP channel ($\Delta v' = -1$ for $v' \leq 43$, $\Delta v' = -2$ for $v' = 44-47$, and $\Delta v' = -3$ for

TABLE 2: Experimental and Calculated Spectral Blue-Shifts of He−$^{79}Br_2$ (B, v') with the Present Potential Surface[a]

			blue-shift (cm^{-1})		
v'	$E_{v'}$ [b] (cm^{-1})	E_{res}^{calc} (cm^{-1})	this work	exptl[c]	exptl[d]
8	−2545.19	−13.814	3.76	3.72 ± 0.05	
10	−2278.34	−13.777	3.80	3.86 ± 0.05	
11	−2150.71	−13.757	3.82		3.74 ± 0.03
12	−2026.96	−13.736	3.84	3.90 ± 0.05	
16	−1571.22	−13.646	3.93	3.95 ± 0.07	
20	−1180.05	−13.544	4.03	4.08 ± 0.08	
24	−853.89	−13.431	4.14	4.21 ± 0.18	4.25 ± 0.03
25	−782.36	−13.401	4.17		4.27 ± 0.03
26	−714.80	−13.372	4.20	4.38 ± 0.20	
30	−482.05	−13.261	4.31	4.40 ± 0.26	
33	−344.43	−13.225	4.35		4.48 ± 0.03
34	−305.09	−13.229	4.34	4.55 ± 0.21	
35	−268.76	−13.246	4.33	4.36 ± 0.22	4.51 ± 0.03
36	−235.43	−13.276	4.30	4.27 ± 0.15	
37	−204.91	−13.322	4.25	3.98 ± 0.10	4.76 ± 0.03
38	−177.14	−13.388	4.18	4.00 ± 0.21	4.85 ± 0.03
39	−151.98	−13.479	4.09	3.97 ± 0.20	
40	−129.29	−13.596	3.98	3.99 ± 0.21	
41	−108.99	−13.754	3.82	3.42 ± 0.30	
42	−90.94	−13.942	3.63	3.87 ± 0.27	
43	−75.02	−14.186	3.39	3.49 ± 0.26	
44	−61.07	−14.453	3.12	3.15 ± 0.31	
45	−49.00	−14.768	2.80	2.47 ± 0.31	
46	−38.67	−15.027	2.55	2.86 ± 0.31	
47	−29.89	−15.159	2.41	2.35 ± 0.31	
48	−22.60	−15.000	2.57	2.44 ± 0.31	

[a] The calculated He−$^{79}Br_2$ (B, v') ground resonance energies (relative to the initial $^{79}Br_2$ vibrational energy level $E_{v'}$) are listed in the third column. [b] $E_{v'} = 0$ corresponds to separated Br atoms. [c] refs 28 and 29. [d] ref 27.

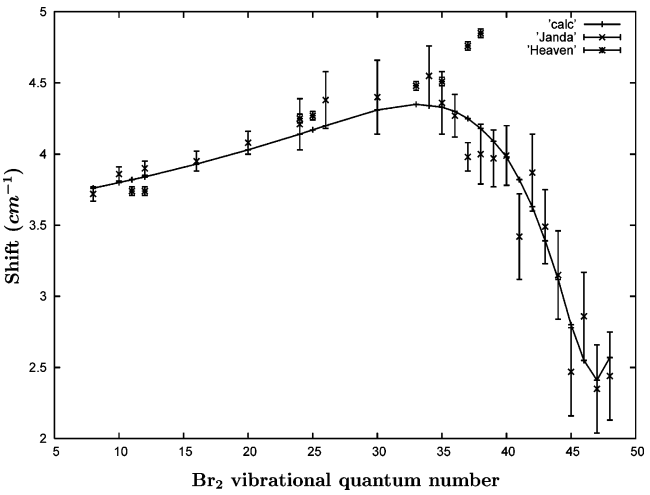

Figure 2. Experimental and calculated spectral blue-shifts of He−$^{79}Br_2$ (B, v') vs the Br_2 vibrational excitation v'. (+) This work; (×) data of Janda and co-workers (refs 28 and 29); (*) data of Heaven and co-workers (ref 27). See the text for details.

$v' = 48$) are shown. The behavior of the calculated and experimental blue-shifts with v' is displayed in Figure 2.

The calculated blue-shifts reproduce nicely the behavior found experimentally, namely an increase of the shift up to $v' \approx 33$ and then a trend inversion leading to a decrease of the blue-shift for higher v' excitations. Actually, the agreement with experiment is nearly quantitative, since the calculated values typically fall within the experimental error bars or close to their limits. It is also stressed that the level of agreement with the data is rather homogeneous in the whole $v' = 8-48$ range (i.e., the blue-shift is reproduced for high v' excitations with an accuracy similar to that for low and intermediate v' levels.

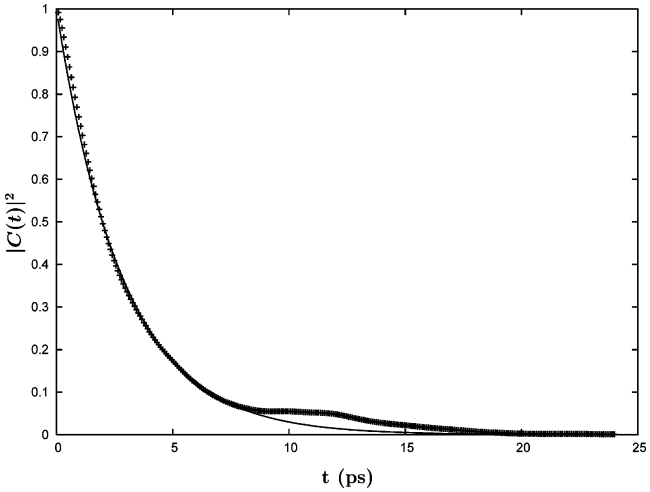

Figure 3. Calculated decay curve of the He−$^{79}Br_2$ (B, $v' = 41$) ground resonance state (+) and the corresponding exponential fit (solid line) vs time.

For $v' < 35$, the current blue-shifts are similar to those obtained in ref 30, as expected because of the above-mentioned similarities between the present and earlier[30] empirical potentials for $r < 4$ Å. Increasing differences appear for $v' > 35$. In this sense, a major qualitative difference is that the theoretical shifts of Figure 2 do not reproduce the oscillatory pattern obtained with the empirical[30] and DIM[33] surfaces for $v' > 40$. It should be noted that, taking into account the experimental error bars, it is unclear whether an oscillatory behavior is actually present in the data, at least as strongly marked as that obtained with the surfaces of refs 30 and 33.

Table 2 shows two additional spectroscopic features which are predicted by the present surface in agreement with the experimental findings.[28] One of them is the closing of the $\Delta v' = -1$ dissociation channel for $v' = 44$. The other feature is the binding energy of He−$^{79}Br_2$ (B, $v' = 44$), found to be D_0(B, $v' = 44$) = 14.453 cm^{-1}, while the experimental estimate is 13.5 ± 1.0 cm^{-1}.

B. Vibrational Predissociation Line Widths. The calculation of the He−Br_2 (B) VP lifetime by fitting the square of the wave packet autocorrelation function, $P(t) = |C(t)|^2$, to a single-exponential function $e^{-t/\tau}$ assumes that an isolated resonance state of the complex is initially prepared by optical excitation. Actually, this is the situation found for $v' < 39$. However, for $v' \geq 39$, the ground resonance state of He−$^{79}Br_2$ (B, v') initially excited is found to interact appreciably with other metastable states energetically close, which belong to vibrational manifolds $v < v'$. Such an interaction of the resonance of interest with other $v < v'$ metastable states was also found in previous calculations,[30] and it complicates the description and analysis of the He−Br_2 (B, v') predissociation dynamics in the high v' region. The initial wave packet populates mainly the resonance state of interest, but also other $v < v'$ resonances close in energy. As a result, after an initial decay, the $P(t)$ curve displays one or more bumps or recurrences, which reflect the decay dynamics of the interacting metastable states. This is illustrated in Figure 3 for the case of He−Br_2 (B, $v' = 41$). It is no longer possible to fit such a decay curve to a single-exponential function.

To obtain the predissociation lifetime corresponding to the resonance of interest for $v' \geq 39$, the following strategy was adopted. It is assumed that in the absence of interaction the recurrences would not appear (they actually do not appear for an isolated resonance) and that the initial decay of $P(t)$ is essentially the decay of the resonance under study. Thus, the

TABLE 3: Experimental Vibrational Predissociation Line Widths and Calculated Lifetimes and Line Widths of He−$^{79}Br_2$ (B, v') with the Present Potential

		line width (cm^{-1})		
v'	τ^{calc} (ps)	this work	exptl[a]	exptl[b]
8	235.0	0.023	0.037	
10	149.5	0.036	0.038	
12	106.8	0.050	0.062	
16	52.7	0.101		
20	28.4	0.187		
24	18.6	0.285		0.16 ± 0.02
25	12.8	0.415		0.20 ± 0.02
28	12.0	0.442		
30	9.7	0.547		
32	7.9	0.672		
34	5.5	0.965	1.00 ± 0.28	
35	4.9	1.083		0.85 ± 0.1
36	4.3	1.235	1.17 ± 0.28	
37	4.0	1.327		1.00 ± 0.2
38	3.6	1.475		1.50 ± 0.3
39	3.5	1.517	1.28 ± 0.28	
41	2.9	1.831	1.57 ± 0.20	
42	2.6	2.042	1.71 ± 0.20	
43	2.4	2.212	1.80 ± 0.20	
44	2.2	2.413	2.93 ± 0.31	
45	2.5	2.124	1.50 ± 0.21	
46	2.4	2.212	1.86 ± 0.20	

[a] refs 28 and 29. [b] refs 27 and 39.

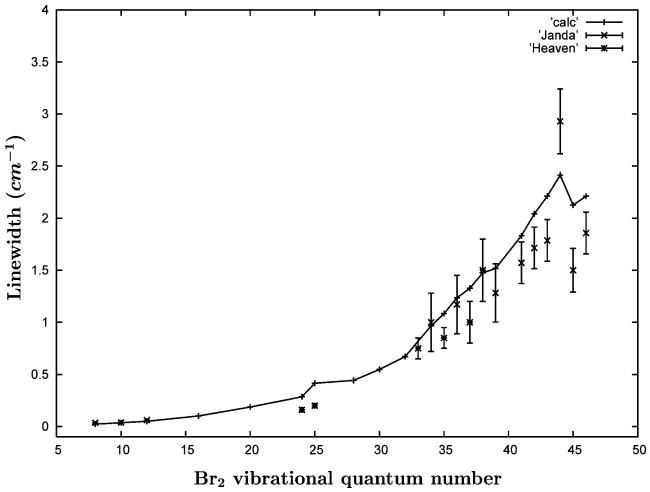

Figure 4. Experimental and calculated predissociation line widths of He−$^{79}Br_2$ (B, v') vs the Br_2 vibrational excitation v'. (+) This work; (×) data of Janda and co-workers (refs 28 and 29); (*) data of Heaven and co-workers (refs 27 and 39).

initial decay of $P(t)$, neglecting the recurrences, is fitted to a single exponential, as shown in Figure 3, and from that fit, the desired lifetime is extracted. The estimate of the lifetime for $v' \geq 39$ made in this way is expected to be somewhat less precise than for low and intermediate v' excitations. The lifetimes and associated line widths calculated for He−$^{79}Br_2$ (B, v') are presented in Table 3, along with the experimental line widths with the reported errors. The calculated and measured line widths are also plotted in Figure 4 for the sake of visual clarity.

Similarly to the case of the spectral shift, the vibrational dependence of the VP line width is reproduced by the present empirical surface in very good agreement with the data, in the whole range of v' excitations probed. A quantitative level of description, typically within experimental error, is achieved for the line widths corresponding to $v' \leq 42$. For $v' = 43-46$, while somewhat lower accuracy is obtained, the experimental behavior is still reproduced, namely, the maximum of the width occurring for $v' = 44$ where the $\Delta v' = -1$ dissociation channel closes, then a decrease for $v' = 45$, followed by a new rising of the width for $v' = 46$.

By comparing the present line widths with those obtained with the empirical surface of ref 30, they are again found to be similar (the current widths being slightly lower) up to $v' \approx 36$, as in the case of the blue-shifts. For higher v' states, the present description of the line widths is substantially improved, particularly in the region $v' > 42$ where the widths of ref 30 were greatly underestimated. It is noted that, except for the oscillation observed experimentally between $v' = 44$ and $v' = 46$, the theoretical line widths of Figure 4 do not reproduce an oscillatory behavior similar to that found for $v' > 40$ in the earlier calculations.[30] This is in agreement with the absence of an oscillatory pattern in the calculated blue-shifts of Figure 2.

TABLE 4: Calculated Br_2 Fragment Rotational State Distributions for the $v' - 1$ and $v' - 2$ Dissociation Channels in the Case $v' = 10$[a]

	population (%)		
j	$v' - 1$	$v' - 2$	$v' - 1$ (exptl)[a]
0	27.22	24.31	5.0 ± 20.0
2	29.02	26.52	29.0 ± 10.0
4	17.86	17.26	34.6 ± 4.2
6	8.29	10.07	15.6 ± 11.5
8	6.57	10.23	8.3 ± 3.6
10	6.10	7.26	10.0 ± 4.2
12	3.43	2.74	
14	1.21	0.86	
16	0.26	0.45	
18	0.05	0.22	
20	<0.01	0.05	

[a] The measured distribution for the $v' - 1$ channel is listed in the fourth column. [b] Taken from ref 32.

C. Product State Distributions. Analysis of the vibrational distributions of the Br_2 (B, $v < v'$) product show that the $\Delta v' = -1$ dissociation channel is dominant for vibrational excitations $v' \leq 42$. As an example, for $v' = 38$, the populations found are 68.3%, 23.9%, and 7.8% for $\Delta v' = -1$, -2, and -3, respectively, which are similar to those obtained for this vibrational level with the empirical potential of ref 30. The $\Delta v' = -1$ channel is energetically closed for $v' \geq 44$. In turn, the population of the $\Delta v' = -2$ channel increases gradually, becoming dominant for $v' > 42$. At these high v' states, the populations of the $\Delta v' = -4$ and -5 dissociation channels are also found to be significant.

Rotational distributions of the Br_2 (B, $v < v'$, j) product fragment were calculated (for even j) with the present potential surface. Table 4 shows such distributions for the $\Delta v' = -1$ and -2 channels in the case of $v' = 10$. The distributions of Table 4 are pratically the same as those obtained for $v' = 10$ in ref 30 (see Table 4 of that work). The present and previous[30] theoretical rotational distributions for the $\Delta v' = -1$ channel agree reasonably well with the corresponding experimental distribution[32] reported for $v' = 10$ (also shown in Table 4). In ref 32, the $\Delta v' = -1$ rotational distribution of $v' = 10$ was recalculated with the same empirical potential of ref 30, now including thermal averaging over transitions involving $J > 0$ states of the complex. Although the comparison with experiment improved (see Figure 4a of ref 32), the calculated rotational distribution did not change much upon thermal averaging. This seems to indicate that for low v' excitations thermal averaging has a rather limited effect on the description of the rotational distributions.

On the contrary, it was shown[32] that, for high v' ($v' \geq 39$), thermal averaging of the calculated rotational distributions is really needed in order to achieve agreement with the measured

TABLE 5: Energies and Positions of the Potential Minima in the Linear ($\theta = 0°$) and Perpendicular ($\theta = 90°$) Configurations of He−Br_2 (B) for Several Br−Br Separations

r (Å)	2.78	3.5	4.0	5.5	7.0	9.0[a]	10.0[a]
V^{min} ($\theta = 0°$)(cm^{-1})	−17.18	−17.06	−17.33	−20.03	−24.74	−19.72 (−26.51)	−17.49 (−18.75)
V^{min} ($\theta = 90°$)(cm^{-1})	−33.46	−33.82	−34.52	−40.02	−49.48	−25.89	−11.94
R^{min} ($\theta = 0°$)(Å)	5.29	5.66	5.91	6.73	7.44	8.41 (0.43)	8.91 (1.07)
R^{min} ($\theta = 90°$)(Å)	3.65	3.50	3.36	2.88	1.81	0.0	0.0

[a] The numbers in parentheses for $r = 9.0$ and 10.0 Å correspond to the absolute potential minimum in the linear configuration. See the text for details.

distributions. The rotational distributions calculated here for high v' levels present similar deviations from the data to those found in earlier simulations[30,32] when thermal averaging is not carried out. It is believed that such discrepancies are due to the limitations of the present dynamical calculations (which assume $J = 0$ and do not consider thermal averaging), rather than to the potential surface.

D. Features of the Potential Surface. The agreement of the present blue-shifts and line widths with the experimental ones, particularly as the Br−Br separation increases, indicates that the dependence on this separation and the three-body interaction effects involved are described well in the interaction potential proposed here. At this point, it is interesting to analyze in more detail how the potential surface changes with the Br−Br bond length. The energy and position of the potential minimum in the linear ($\theta = 0°$) and perpendicular ($\theta = 90°$) configurations of He−Br_2 (B) are listed in Table 5 for several Br−Br distances. In addition, contour plots of the potential surface are shown in Figures 5 and 6 for six different Br−Br bond lengths.

In the linear configuration, at $r = 2.78$ Å (which is the average Br−Br distance in the $v' = 8$ state), the minimum energy is −17.18 cm^{-1} at $R^{min} = 5.29$ Å. Between $r = 2.78$ Å and $r = 4.0$ Å, V^{min} ($\theta = 0°$) decreases slightly, and then, it increases monotonically for $r \geq 4.0$ Å up to $r \approx 7.0$ Å. For larger r distances, V^{min} ($\theta = 0°$) gradually decreases, approaching the value corresponding to the well depth of the He−Br interaction. The position of the potential minimum, R^{min} ($\theta = 0°$), increases monotonically with r in the entire range of Br−Br bond lengths.

Interestingly, for large r distances ($r \geq 9.0$ Å), there appears in the linear geometry an additional, deeper energy minimum at short R^{min} ($\theta = 0°$) distances. In the cases of $r = 9.0$ and 10.0 Å, the minima are V^{min} ($\theta = 0°$) = −26.51 and −18.75 cm^{-1} at R^{min} ($\theta = 0°$) = 0.43 and 1.07 Å, respectively (the values in parentheses in Table 5). These energy minima become the absolute potential minima. For those large r separations, the interaction of He with the Br atoms is optimal (even stronger than in the perpendicular configuration) when He is between the two Br atoms, but somewhat closer to one of them.

In the perpendicular configuration, the minimum of energy remains rather constant (increasing only slightly) up to $r \approx 4.0$ Å. Then, V^{min} ($\theta = 90°$) increases more rapidly up to ∼50 cm^{-1} for $r \approx 7.0$ Å. For larger r distances, V^{min} ($\theta = 90°$) gradually decreases, reaching the value −11.94 cm^{-1} for $r = 10.0$ Å, which is lower than the well depth of the He−Br pairwise interaction, and then the two V^{min} ($\theta = 0°$) values for $r = 10.0$ Å. For such large Br−Br separations, the He atom is not able to interact effectively with the two Br atoms in the perpendicular configuration, and the linear configuration of He−Br_2 (B) becomes more stable than the T-shaped one. The R^{min} ($\theta = 90°$) position of the potential minimum decreases monotonically with increasing r, to the extent that, for $r > 7.5$ Å, $R^{min} = 0$ Å, and the He atom is placed in the middle of the Br−Br bond distance. It is noted that the same result was found with the DIM surface of ref 33. Thus, for $r > 7.5$ Å, the most stable configuration of He−Br_2 (B) becomes the linear one with the He atom between the two Br atoms, either in the middle of the Br−Br bond or somewhat closer to one of the Br atoms.

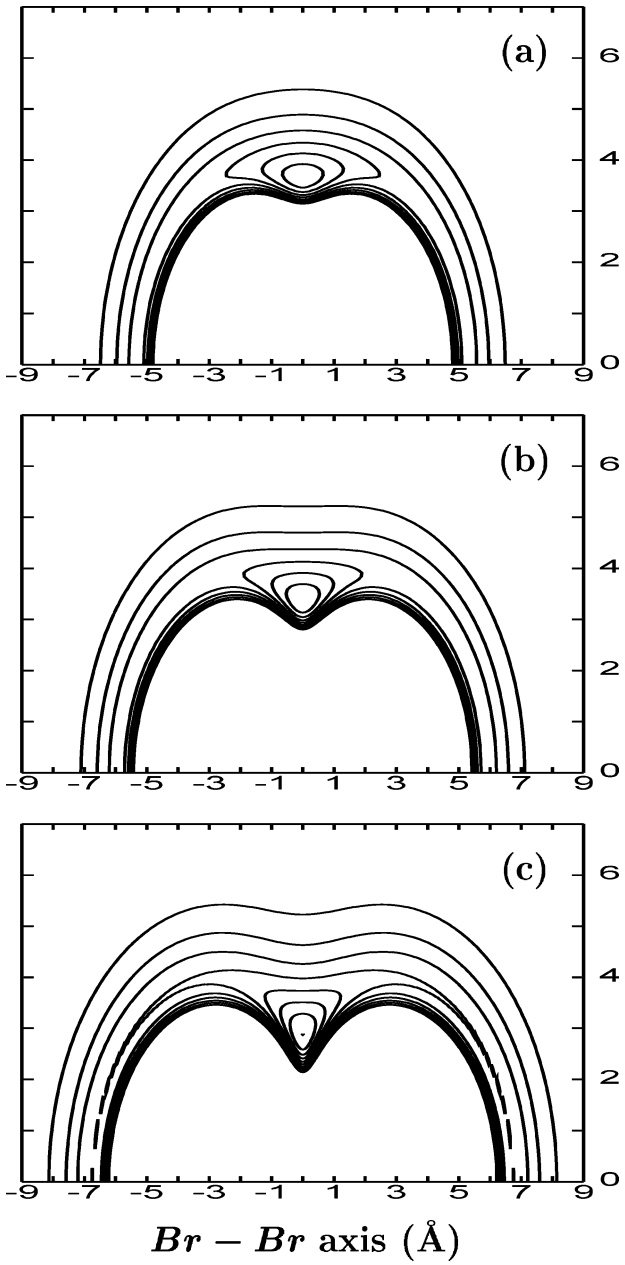

Figure 5. Contour plots of the He−Br_2 (B) empirical potential surface for three Br−Br separations: $r = 2.78$ Å (a), $r = 4.0$ Å (b), and $r = 5.5$ Å (c). Spacing between the contours is 5 cm^{-1} starting from the outermost contour at −5 cm^{-1}, and the units are Å on both axes of the plot. For $r = 2.78$, 4.0, and 5.5 Å, the Br atoms are located at ±1.39 Å, ±2.0 Å, and ±2.75 Å, respectively, on the horizontal axis of the plot.

The present empirical surface can be compared with the ab initio calculations of the He−Br_2 (B) surface reported in ref 35 for the Br−Br separations $r = 2.4485$, 2.6776, and 3.0862 Å.

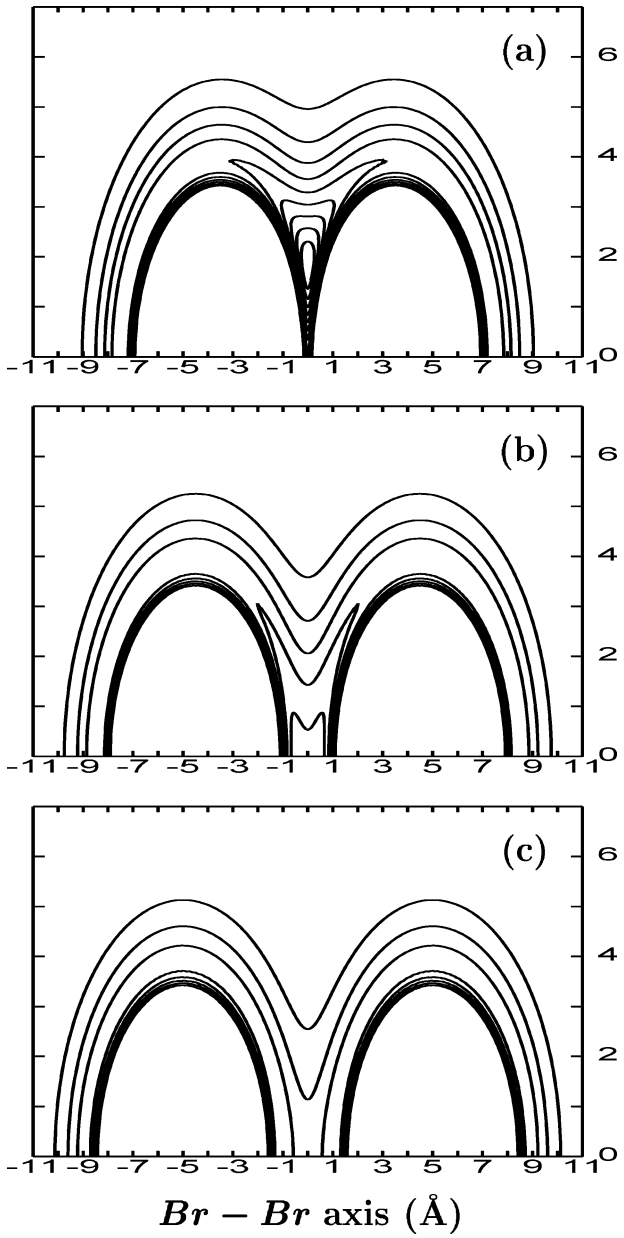

Figure 6. Same as Figure 5 but for the Br−Br separations $r = 7.0$ Å (a), $r = 9.0$ Å (b), and $r = 10.0$ Å (c), for which the Br atoms are located at ±3.5 Å, ±4.5 Å, and ±5.0 Å, respectively, on the horizontal axis of the plot.

In the perpendicular configuration, the empirical/ab initio comparisons for V^{min} and R^{min} are $V^{min} = -33.40/-34.35$ cm^{-1}, $-33.44/-32.29$ cm^{-1}, and $-33.56/-30.79$ cm^{-1} and $R^{min} = 3.71/3.68$ Å, 3.67/3.70 Å, and 3.59/3.66 Å for the distances $r = 2.4485$, 2.6776, and 3.0862 Å, respectively (see Table 8 of ref 35). In the linear configuration, the comparisons are $V^{min} = -17.45/-17.59$ cm^{-1}, $-17.24/-20.58$ cm^{-1}, and $-17.06/-21.59$ cm^{-1} and $R^{min} = 5.12/5.16$ Å, 5.24/5.17 Å, and 5.45/5.32 Å for the same three Br−Br separations. Thus, a good agreement is found between the empirical surface and the ab initio calculations for the energy minima and equilibrium positions of the He−Br_2 (B) potential.

The contour plots of the potential of Figures 5 and 6 show clearly the deepening of the absolute minimum V^{min} ($\theta = 90°$) as He approaches the middle of the Br−Br internuclear axis when r increases up to $r \approx 7$ Å. Figure 6b,c shows that the situation changes for very large r ($r \geq 9.0$ Å), and the interaction is now stronger at configurations different than the perpendicular one. The slight increase of V^{min} ($\theta = 90°$) for $r < 4.0$ Å is consistent with the smooth increase found for the spectral blue-shift between $v' = 8$ and $v' \approx 35$. The deepening of the absolute potential minimum in the range $4.0 < r < 7.0$ Å, due to three-body interaction effects, is also consistent with an increasing strength of the vdW bond and with the sharp decrease of the blue-shift found for the levels $35 \leq v' \leq 48$. Similarly, the experimental (and calculated) line width increases slowly from $v' = 8$ to $v' \approx 35$, while the increase is appreciably more pronounced for $v' > 35$ (see Figure 4). As in the case of the blue-shifts, this behavior of the line width can be correlated with the behavior of the potential well depth with r, being rather constant for $r < 4.0$ Å and then increasing for $4.0 < r < 7.0$ Å. At present, there are no experiments for $v' > 48$, probing the region of large Br−Br separations $r > 7.0$ Å.

The present potential surface suggests the following picture from the electrostatic point of view. For low and intermediate v' states (corresponding to distances $r < 3.5-4.0$ Å), the He atom is relatively far away from the Br_2 subunit, and the electronic density of the Br atoms lies essentially along the diatomic internuclear axis, in the Br−Br covalent bond. In this situation, the He−Br_2 (B) intermolecular potential can be reliably described as a sum of two-body He−Br interactions. As the Br−Br bond length increases, He approaches the middle position of the Br−Br bond to achieve an optimal interaction with the Br atoms. As a consequence of this approach, the electronic density shared between the Br atoms and He increases, giving place to an increasingly attractive three-body interaction. Such a three-body interaction stabilizes the complex, leading to a strengthening of the vdW bond, which is reflected in the decrease of the spectral blue-shift with increasing v'. As r increases further ($r > 7.0$ Å), the vdW bond becomes gradually weaker, and the intermolecular potential approaches the asymptotic limit of a single He−Br interaction. Calculations of electronic density maps of He−Br_2 (B) for different Br−Br bond lengths would be very helpful to test the above picture.

IV. Conclusions

An empirical interaction potential surface for the He−Br_2 ($B^3\Pi_u$) complex is proposed in this work. The intermolecular He−Br_2 potential is represented by a sum of pairwise He−Br Morse interactions, plus a three-body interaction term. The parameters of the potential surface are fitted in order to reproduce the spectral blue-shifts and vibrational predissociation line widths measured in the range $v' = 8-48$ of Br_2 vibrational excitations. The blue-shifts and line widths obtained with the fitted surface are in very good agreement with the data (typically within experimental error or close to its limits) in all the v' range probed experimentally. It is remarkable to observe the good level of description provided by the interaction potential for $v' > 35$ as compared to surfaces previously reported. The region of high Br_2 vibrations is particularly difficult to describe, since the dependence of the He−Br_2 (B) potential on the Br−Br separation becomes stronger as this separation increases.

Analysis of the potential surface shows that for most of the range of Br−Br bond lengths, the most stable He−Br_2 (B) configuration is the T-shaped one. When the Br_2 bond elongates from low to high distances (up to ∼7.5 Å), the He atom approaches the middle position between the two Br atoms, and the vdW bond becomes gradually stronger because of an increasingly attractive three-body interaction, consistent with the experimental finding. For larger diatomic separations, the vdW bond increasingly weakens, and the most stable geometry of the complex becomes linear, with He between the Br atoms,

either in the middle of the Br−Br bond (for diatomic distances between 7.5 Å and ∼9.0 Å) or somewhat closer to one Br atom (for Br−Br bond lengths ≥ 9.0 Å).

Finally, the model applied to characterize the $He-Br_2$ (B) potential surface as a sum of pairwise interactions plus a three-body term has proven successful, and it appears as a powerful alternative to obtain potential energy surfaces of other vdW complexes in the absence of accurate ab initio calculations. It would be very interesting to test the present potential surface in the region of large Br−Br separations with the aid of high-quality ab initio calculations.

Acknowledgment. This work was supported by C.I.C.Y.T. (Ministerio de Educación y Ciencia), Spain, grant FIS-2004-02461. The Centro de Supercomputación de Galicia (CESGA), and the Grupo de SuperComputación del CIEMAT (GSC) are acknowledged for allocation of computer time.

References and Notes

(1) Smalley, R. E.; Levy, D. H.; Warton, L. *J. Chem. Phys.* **1976**, *64*, 3266.
(2) Smalley, R. E.; Warton, L.; Levy, D. H. *J. Chem. Phys.* **1978**, *68*, 671.
(3) Beswick, J. A.; Jortner, J. *J. Chem. Phys.* **1978**, *69*, 512.
(4) Sharfin, W.; Johnson, K. E.; Warton, L.; Levy, D. H. *J. Chem. Phys.* **1979**, *71*, 1292.
(5) Kenny, J. E.; Johnson, K. E.; Sharfin, W.; Levy, D. H. *J. Chem. Phys.* **1980**, *72*, 1109.
(6) Kenny, J. E.; Russel, T. D.; Levy, D. H. *J. Chem. Phys.* **1980**, *72*, 3607.
(7) Valentini, J. J.; Cross, J. B. *J. Chem. Phys.* **1982**, *77*, 572.
(8) García-Vela, A.; Villarreal, P.; Delgado-Barrio, G. *J. Chem. Phys.* **1990**, *92*, 6504. García-Vela, A.; Villarreal, P.; Delgado-Barrio, G. *J. Chem. Phys.* **1991**, *94*, 7868.
(9) Willberg, D. M.; Gutmann, M.; Breen, J. J.; Zewail, A. H. *J. Chem. Phys.* **1992**, *96*, 198.
(10) Gutmann, M.; Willberg, D. M.; Zewail, A. H. *J. Chem. Phys.* **1992**, *97*, 8037.
(11) Burroughs, A.; Heaven, M. C. *J. Chem. Phys.* **2001**, *114*, 7027.
(12) Burroughs, A.; Kerenskaya, G.; Heaven, M. C. *J. Chem. Phys.* **2001**, *115*, 784.
(13) García-Vela, A. *J. Phys. Chem. A* **2002**, *106*, 6857.
(14) Cline, J. I.; Evard, D. D.; Thommen, F.; Janda, K. C. *J. Chem. Phys.* **1985**, *84*, 1165.
(15) Evard, D. D.; Bieler, C. R.; Cline, J. I.; Sivakumar, N.; Janda, K. C. *J. Chem. Phys.* **1988**, *89*, 2829.
(16) Cline, J. I.; Reid, B. P.; Evard, D. D.; Sivakumar, N.; Halberstadt, N.; Janda, K. C. *J. Chem. Phys.* **1988**, *89*, 3535.
(17) Cline, J. I.; Sivakumar, N.; Evard, D. D.; Bieler, C. R.; Reid, B. P.; Halberstadt, N.; Hair, S. R.; Janda, K. C. *J. Chem. Phys.* **1989**, *90*, 2605.
(18) (a) Gray, S. K.; Wozny, C. E. *J. Chem. Phys.* **1989**, *91*, 7671. (b) Gray, S. K.; Wozny, C. E. *J. Chem. Phys.* **1991**, *94*, 2817.
(19) Williams, J.; Rohrbacher, A.; Seong, J.; Marianayagam, N.; Janda, K. C.; Burcl, R.; Szczęśniak, M. M.; Chalasiński, G.; Cybulski, S. M.; Halberstadt, N. *J. Chem. Phys.* **1999**, *111*, 997.
(20) Bastida, A.; Miguel, B.; Zúñiga, J.; Requena, A.; Halberstadt, N.; Janda, K. C. *J. Chem. Phys.* **1999**, *111*, 4577.
(21) Hernández, M. I.; Halberstadt, N.; Sands, W. D.; Janda, K. C. *J. Chem. Phys.* **2000**, *113*, 7252.
(22) García-Vela, A. *J. Chem. Phys.* **2003**, *119*, 5583.
(23) García-Vela, A. *J. Chem. Phys.* **2005**, *122*, 14312.
(24) Skene, J. M.; Lester, M. I. *Chem. Phys. Lett.* **1985**, *116*, 93.
(25) Drobits, J. C.; Lester, M. I. *J. Chem. Phys.* **1988**, *89*, 4716.
(26) Waterland, R. L.; Lester, M. I.; Halberstadt, N. *J. Chem. Phys.* **1990**, *92*, 4261.
(27) van de Burgt, L. J.; Nicolai, J.-P.; Heaven, M. C. *J. Chem. Phys.* **1984**, *81*, 5514.
(28) Jahn, D. G.; Clement, S. G.; Janda, K. C. *J. Chem. Phys.* **1994**, *101*, 283.
(29) Jahn, D. G.; Barney, W. S.; Cabalo, J.; Clement, S. G.; Rohrbacher, A.; Slotterback, T. J.; Williams, J.; Janda, K. C.; Halberstadt, N. *J. Chem. Phys.* **1996**, *104*, 3501.
(30) González-Lezana, T.; Hernández, M. I.; Delgado-Barrio, G.; Buchachenko, A. A.; Villarreal, P. *J. Chem. Phys.* **1996**, *105*, 7454.
(31) Nejad-Sattari, M.; Stephenson, T. A. *J. Chem. Phys.* **1997**, *106*, 5454.
(32) Rohrbacher, A.; Ruchti, T.; Janda, K. C.; Buchachenko, A. A.; Hernández, M. I.; González-Lezana, T.; Villarreal, P.; Delgado-Barrio, G. *J. Chem. Phys.* **1999**, *110*, 256.
(33) Buchachenko, A. A.; González-Lezana, T.; Hernández, M. I.; de Lara Castells, M. P.; Delgado-Barrio, G.; Villarreal, P. *Chem. Phys. Lett.* **2000**, *318*, 578.
(34) Valdés, A.; Prosmiti, R.; Villarreal, P.; Delgado-Barrio, G. *Mol. Phys.* **2004**, *102*, 2277.
(35) de Lara Castells, M. P.; Buchachenko, A. A.; Delgado-Barrio, G.; Villarreal, P. *J. Chem. Phys.* **2004**, *120*, 2182.
(36) Barrow, R. F.; Clark, T. C.; Coxon, J. A.; Yee, K. K. *J. Mol. Spectrosc.* **1974**, *51*, 428.
(37) Engel, V. *Chem. Phys. Lett.* **1992**, *189*, 76.
(38) Ceotto, M.; García-Vela, A. *J. Chem. Phys.* **2001**, *115*, 2146.
(39) The lifetimes reported in ref 27 were half of the actual lifetimes, as noted in ref 28.